Chemical Engineering Journal 164 (2010) 393–402

Contents lists available at ScienceDirect

Chemical Engineering Journal

journal homepage: www.elsevier.com/locate/cej

Modelling of particle motion in an internal re-circulatory fluidized bed

Kevin Cronin[a,*], Muammer Çatak[a], Dario Tellez-Medina[a], Vincent Cregan[b], Stephen O'Brien[b]

[a] Department of Process & Chemical Engineering, University College Cork, Ireland
[b] Macsi, Department of Mathematics & Statistics, University of Limerick, Ireland

ARTICLE INFO

Article history:
Received 28 September 2009
Received in revised form 24 February 2010
Accepted 2 March 2010

Keywords:
Re-circulatory fluidized bed
Particle motion
Theoretical expressions
Drag coefficient
Granulation

ABSTRACT

Fluidized bed technology is commonly used in the pharmaceutical industry for the production of granules. One common arrangement is where a systematic circulatory motion is superimposed on the random fluid bed motion of the particles by controlling the air flow pattern in the system. The fluidized particles travel up an inner tube (known as a riser), exit out the top into the main chamber, then fall down the annular space between the tube and the chamber and then repeat the process. This paper describes the development of an analytical model of particle motion incorporating particle weight and a turbulent air drag force. The model is valid for spherical and non-spherical granules. The model provides a theoretical description of the velocity and displacement of the particles and hence the magnitude of the residence times in the various zones of the system. Its output is validated against experimentally recorded displacement versus time histories of the particles from two fluidized bed systems. Studies with the model are used to suggest parameters by which the granulation characteristics of a re-circulatory system can be assessed.

1. Introduction

Fluidized bed technology is commonly used for drying, heating, cooling, granulation and coating of powder or granular materials. For the case of granulation, the technology is available in a number of process configurations (batch or continuous, circulatory or non-circulatory, etc.). One common arrangement is where a systematic internal circulatory motion is superimposed on the random fluid bed motion of the particles by controlling the air flow pattern in the system. The fluidized particles travel up an inner or draught tube, exit out the top into the main chamber (the sprouting zone), then fall down the annular space between the tube and the chamber to the base of the unit and then repeat the process. A liquid binder is sprayed over the particles as they pass through the inner tube to wet their surfaces so they can stick together if they come in contact. Repeated movement of the particles through the spray zone results in agglomeration of particles to form granules. Fig. 1 illustrates such a system.

The initial population of the solid material may consist of unit or individual particles of known size and shape. As the granulation process advances in time, the particles agglomerate to form granules and their size, shape and composition distributions becomes more heterogeneous. Note for this work, the term particles may be used to mean both individual unit particles and agglomerations of these (i.e. granules). One fundamental property of the particles is their velocity and consequent displacement versus time history. Velocity informs most of the sub-processes of granulation including the probability of contact with liquid binder droplets in the spray zone, the drying rate of the wet film on the particles when they exit the spray zone (through its effect on the Reynolds number), the collision probability with other particles or granules and the probability of subsequent coalescence (through the Stokes number) [1,2]. Furthermore knowledge of velocity enables the residence time of the particles in each distinct zone (such as the spray zone) of the granulator to be quantified and the average circulation time for the particles, i.e. the time required to complete one circulation of the system to be found [3]. The object of this paper is to develop and validate analytical and numerical models of particle velocity and displacement in an internal re-circulatory fluidized bed granulator. These are then used to calculate characteristic residence and recirculation times and other process characteristics. The chosen approach is deterministic and does not consider random variability in such systems as described by Harris et al. [4]. Output from the models is then used to characterize system behaviour and to identify relationships between granule size and aggregation rates.

2. Theory

2.1. Air flow pattern model

Fluid drag force usually makes a significant contribution to particle motion and so knowledge of the air flow pattern in the system

* Corresponding author.
E-mail address: k.cronin@ucc.ie (K. Cronin).

1385-8947/$ – see front matter © 2010 Elsevier B.V. All rights reserved.
doi:10.1016/j.cej.2010.03.008

Nomenclature

A_S	surface area of a particle [m^2]
A_p	projected area of a particle [m^2]
C_D	drag coefficient [–]
c_T	drag factor [kg/m]
d	particle diameter [m]
d_e	particle equivalent diameter [m]
F_D	drag force [N]
h_1	height of inner tube [m]
h_2	(maximum) height of particle above inner tube [m]
K_1	Stokes shape factor [–]
K_2	Newton shape factor [–]
m	particle mass [kg]
Re	Reynolds number [–]
T	circulation time [s]
t	time [s]
u_P	particle velocity [m/s]
u_F	fluid velocity [m/s]
u_T	terminal velocity [m/s]
V	particle volume [m^3]
x_B	binder material mass fraction [–]
y	particle displacement [m]
ρ	granule (average) density [kg/m^3]
ρ_F	fluid density [kg/m^3]
ρ_B	binder material density [kg/m^3]
ρ_P	unit particle density [kg/m^3]
μ_F	fluid viscosity [Pa s]
φ	particle sphericity [–]
ε	particle porosity [–]

is necessary. To permit the formulation of analytical solutions, a simpler geometry than usually prevails is examined; the system consists of an inner cylindrical tube concentrically located inside a larger diameter and taller outer cylindrical main tube. Air is blown vertically up through both tubes and using a flow distributor it is arranged that there is a certain air velocity in the inner tube and a lower air velocity in the annular space between the inner and outer tube. Air velocity in the outer annular zone is solely in the vertical direction with no radial component. Moreover air velocity is uniform across the flow cross-section (except very close to the walls) Air velocity in the inner tube displays these same characteristics. The air velocity in the space above the inner tube within the main tube has a more complex distribution. The high speed air emanating from the top of the inner tube expands to form a conical jet. The lower speed air moving up from the annular space is constrained to the perimeter zone of the main tube. Air velocity in the main tube above the riser is thus demarcated into two regions; a central region of increasing radius which contains a fast but decelerating air stream surrounded by a thinning annular region of a slow but constant velocity. In this central region, the air has a small radial component of velocity. At some height above the top of the inner tube, both streams merge as one and flow within the main tube becomes uniform. For this work, the air flow velocity in the central region of the main tube (above the inner tube) will be characterized by a single axial velocity.

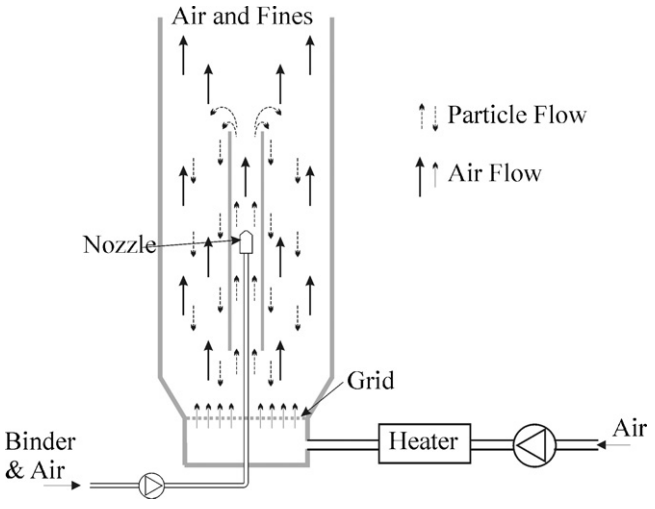

Fig. 1. Internal re-circulatory fluidized bed granulator.

Compartmentalising the real flow system into zones is to an extent arbitrary and a variety of approaches are possible [3]. For this work, it is taken that there are three distinct flow zones through which the particle sequentially passes through in its re-circulatory motion. The particle is assumed to start from rest on the air distributor grid just below the base of the inner cylinder and is carried upwards inside the inner tube by the drag force from the rapidly moving air. Fluid velocity in this inner tube is denoted u_{F1}. The region inside the inner tube is termed *Zone 1*. The particle exits from the top of the inner tube into a slower moving air stream in the central region of the main tube where it decelerates to zero velocity at some height above the top of the inner tube. This is the maximum elevation, h_{max} that the particle achieves during its motion. Average fluid velocity in this region is u_{F2} and *Zone 2* is the corresponding central region within the main tube. The particle then falls down near the perimeter of the main tube and through the annular space between the inner and outer tubes against the slow upward moving air. Fluid velocity here is u_{F3} and the region is termed *Zone 3*. At the base of this zone, it tumbles into the center at the bottom of the inner tube and the motion re-commences. Note this approach assumes the particle transits from zone 2 to zone 3 at the apogee of its displacement. Furthermore during the motion in zone 2, the particle is also assumed to be carried over laterally towards the side of the main tube. Fig. 2a and b illustrates the specific geometry under consideration, indicating zone boundaries and typical particle trajectory (Fig. 2a) and particle and fluid velocities and trajectory (Fig. 2b).

2.2. Particle kinetics

While in industrial granulators, many millions of particles can be simultaneously circulating, for this paper the focus is on the motion of a single body. In general, particles in a gas flow field may be subject to forces including gravity, fluid drag, buoyancy, particle to particle collisions, particle to wall collisions and inter-particle forces such as Van der Waals, capillary and electrostastic forces. The latter three forces can be neglected for particle sizes greater than 100 μm [5]. As air density is usually three orders of magnitude lower than particle density, buoyancy force can also be ignored [6]. For the very dilute phase systems under analysis here, collision forces have a low probability of occurrence and will also be discounted. There remain only two forces acting on the particle; weight force and drag force from the fluid. Furthermore for the analysis, the particle is taken to have a velocity component solely in the vertical direction and any radial component is ignored, i.e. a one-dimensional kinetic approach is taken. This implies particle trajectory is considered to be in the form of a shallow loop, as indicated in Fig. 2, with the small actual component of displacement in the radial direction ignored.

The particle under analysis can be either a single homogenous spherical particle or an agglomerated granule consists of individual unit particles (glass beads for this work), a solid binder matrix and occluded air in the spaces between the particles. Four parameters

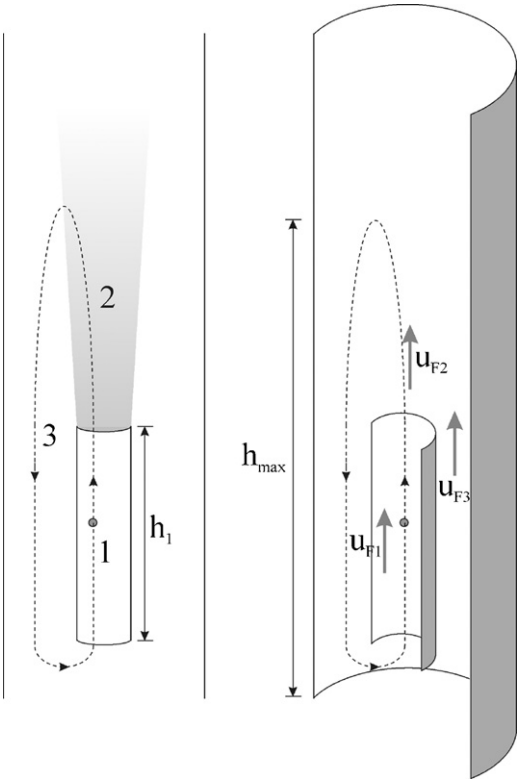

Fig. 2. (a and b) Simplified zone flow geometry.

of such a granule influences its motion; the (average or equivalent) diameter, d_e the shape (measured by sphericity), φ the porosity or void fraction, ε and the mass fraction of binder material present, x_B. Knowing the porosity of the granule and the mass fraction of binder in it, the average density, ρ of the granule can be found given the densities of its components are known. Average granule density and diameter determine the weight force acting on the granule while granule diameter and sphericity inform the drag force on the particle. For a particle with one (axial) degree of freedom, the basic description of the motion comes from the application of Newton's Second Law:

$$F_D - mg = m\frac{d - u_p}{dt} \tag{1}$$

where m is particle mass, u_P is particle velocity and F_D is the drag force acting on the particle. Considering the particle as approximately spherical, its mass will be

$$m = \frac{\pi}{6}d^3\rho \tag{2}$$

where average granule density will depend on porosity, ε, binder mass fraction, x_B and the respective densities of the unit particles ρ_P and binder agent, ρ_B

$$\rho = \frac{1}{(((1 - x_B)/\rho_P) + (x_B/\rho_B))(1 + (\varepsilon/(1 - \varepsilon)))} \tag{3}$$

There are many expressions given in the literature for the drag force exerted on a particle. The force is principally determined by the prevailing flow regime which in turn can be quantified by the Reynolds number. For large Reynolds numbers, the regime can be classified as turbulent where drag force acting on the particle is proportional to the square of its relative velocity in the fluid and the force given by

$$F_D = -c_T(u_P - u_F)|u_P - u_F| \tag{4}$$

where c_T is the turbulent drag factor and u_F is local fluid velocity. The absolute sign is necessary to obtain the correct direction of the drag force irrespective of the direction of u_P and u_F [7]. The turbulent drag factor in turn depends on the drag coefficient C_D, fluid density ρ_F and the projected area of the particle (which is a circle for a spherical particle).

$$c_T = 0.5C_D\rho_F A_p \tag{5}$$

For a sphere, the drag coefficient is uniquely defined by the Reynolds number. Although there are a wide number of competing formulae, a commonly used empirical expression, valid for Reynolds numbers less than 2×10^5 is [8]

$$C_D = \frac{24}{Re}(1 + 0.173Re^{0.657}) + \frac{0.413}{1 + 16300Re^{-1.09}} \tag{6}$$

where Reynolds number is calculated as

$$Re = \frac{\rho_F d(u_P - u_F)}{\mu_F} \tag{7}$$

Note for Reynolds numbers greater in magnitude than 1000, the drag coefficient is almost constant at 0.44. For non-spherical particles, formulae for the drag coefficient are more complicated and depend on the departure from sphericity of the particle in question and the prevailing Reynolds number. Ganser [9] recommends the formula

$$C_D = \frac{24}{ReK_1}(1 + 0.1118(ReK_1K_2)^{0.657}) + \frac{0.4305}{1 + (3305/ReK_1K_2)} \tag{8}$$

where the factors K_1 (Stokes) and K_2 (Newton) are defined using

$$K_1 = \frac{1}{(1/3) + (2/3)(1/\sqrt{\phi})} - 2.25\frac{d}{D}$$

$$K_2 = 10^{1.8148[-\log_{10}\phi]^{0.5743}} \tag{9}$$

Both factors primarily depend on the sphericity of the particle though K_1 also has a dependency on the size ratio of the particle and the containing vessel. The sphericity is defined as the ratio of the surface area of a sphere of equal volume, V with the particle to the surface area of the particle itself. It can be calculated as

$$\phi = \frac{4.836V^{0.666}}{A_S} \tag{10}$$

For non-spherical particles, equivalent diameter, d_e is determined from

$$d_e = \left(\frac{6V}{\pi}\right)^{1/3} \tag{11}$$

2.3. Particle kinematics

An analytical solution to Eq. (1) is only possible by treating the drag coefficient as constant (either at a known magnitude such as 0.44 or a time-averaged value over the duration of interest). Even with this simplification, solutions are complicated by the fact that the particle passes through three distinct zones in the re-circulatory unit, each with its own local fluid velocity. The motion that takes place is very sensitive to the respective magnitudes of particle initial velocity in each zone, u_0, local fluid velocity, u_F and an invariant quantity, the terminal velocity, u_T. This defined as

$$u_T = \sqrt{\frac{mg}{c_T}} \tag{12}$$

Note the drag coefficient (and hence terminal velocity) can be assumed constant for the whole re-circulatory motion or less restrictively constant within each zone. In the latter case, each granule will have three different terminal velocities for each of the

zones, u_{T1}, u_{T2}, u_{T3}. The solution of differential equation (1) using the appropriate initial conditions for each zone yields expressions for particle velocity in each zone. These in turn can be integrated to obtain particle displacement as a function of time.

In zone 1 the particle starts under the base of the inner tube with zero velocity. It is carried up the tube within an air stream of velocity u_{F1}, drag force always exceeds weight force and the particle is continuously accelerated. The expressions for particle velocity and displacement in this zone are respectively:

$$u_p = -u_{T1}\ \coth\left[\frac{g}{u_{T1}}t + \coth^{-1}\left(\frac{u_{F1}}{u_{T1}}\right)\right] + u_{F1} \tag{13}$$

$$y = \int udt = u_{F1}t + \frac{u_{T1}^2}{g}\left\{-\ln\left[\sinh\left\{\frac{g}{u_{T1}}t + \coth^{-1}\left(\frac{u_{F1}}{u_{T1}}\right)\right\}\right]\right\} + \ln\left\{\sinh\left[\coth^{-1}\left(\frac{u_{F1}}{u_{T1}}\right)\right]\right\} \tag{14}$$

This component of the motion is terminated when particle displacement, y equals the height of the inner tube, h_1 and the particle exits out the top. The time required for this motion is t_1, residence time of the particle in the inner tube and is obtained from Eq. (14). The spray nozzle is generally located at some position within the inner tube and thus either the whole inner tube or some fraction of it can be denoted as the spray zone. Using Eq. (14), the residence time in the spray zone can be calculated.

In zone 2, the motion is more complex. The particle enters the zone with initial velocity $u_p(t_1)$. Initially particle velocity is greater than air velocity but as the particle decelerates its velocity falls below local air velocity. Hence at some point the direction of the drag force is reversed. As particle weight always exceeds the (absolute) magnitude of drag force, particle decelerates to zero velocity. There are two sequential expressions for particle velocity and displacement in this zone separated by a switch-over time. The switch-over time, t_S is given as

$$t_S = \frac{u_{T2}}{g}\tan^{-1}\left(\frac{u_{F2} - u_p(t_1)}{u_{T2}}\right) \tag{15}$$

For times shorter than this, particle velocity and displacement are given as:

$$u_p = -u_{T2}\ \tan\left[\frac{g}{u_{T2}}t + \tan^{-1}\left(\frac{u_{F2} - u_p(t_1)}{u_{T2}}\right)\right] + u_{F2} \tag{16}$$

$$y = u_{F2}t + \frac{u_{T2}^2}{g}\left\{\ln\left[\cos\left\{\frac{g}{u_{T2}}t + \tan^{-1}\left(\frac{u_{F2} - u_p(t_1)}{u_{T2}}\right)\right\}\right]\right\} + 0.5\ \ln\left\{1 + \frac{u_{F2} - u_p(t_1)}{u_{T2}}\right\} \tag{17}$$

For times after the switch-over time, the corresponding expressions are:

$$u_p = -u_{T2}\tanh\left[\frac{g}{u_{T2}}t + \tan^{-1}\left(\frac{u_{F2} - u_p(t_1)}{u_{T2}}\right)\right] + u_{F2} \tag{18}$$

$$y = u_{F2}\left[t + \frac{u_{T2}^2}{g}\tan^{-1}\left(\frac{u_{F2} - u_p(t_1)}{u_{T2}}\right)\right] - \frac{u_{T2}^2}{g}\left\{\ln\left[\cosh\left\{\frac{g}{u_{T2}}t + \frac{u_T}{g}\tan^{-1}\left(\frac{u_{F2} - u_p(t_1)}{u_{T2}}\right)\right\}\right]\right\} + \frac{u_{T2}^2}{g}\left\{-\frac{u_{F2}}{u_{T2}}\tanh^{-1}\left(\frac{u_{F2} - u_p(t_1)}{u_{T2}}\right) + 0.5\ln\left(1 + \left(\frac{u_{F2} - u_p(t_1)}{u_{T2}}\right)^2\right)\right\} \tag{19}$$

From Eq. (18), the time required for the particle to achieve zero velocity can be found. This time is denoted t_2 and is the elapsed time from when the particle exited the inner tube. The displacement of the particle at this time $y(t_2)$, which is denoted h_{max} is the maximum height that the particle reaches.

In zone 3 the particle falls down along the inner surface of the main tube and then through the annular space between both tubes against the upward moving air stream with velocity u_{F3}. The initial particle velocity is zero, and the expressions for particle velocity and displacement are respectively:

$$u_p = -u_{T3}\ \tanh\left[\frac{g}{u_{T3}}t + \tanh^{-1}\left(\frac{u_{F3}}{u_{T3}}\right)\right] + u_{F3} \tag{20}$$

$$y = u_{F3}t + \frac{u_{T3}^2}{g}\left\{-\ln\left[\cosh\left\{\frac{g}{u_{T3}}t + \tanh^{-1}\left(\frac{u_{F3}}{u_{T3}}\right)\right\}\right]\right\} + \ln\left\{\cosh\left[\tanh^{-1}\left(\frac{u_{F3}}{u_{T3}}\right)\right]\right\} \tag{21}$$

Using Eq. (21), the time required for the particle to return to the base of the unit (and achieve a displacement of h_{max}) can be found and is denoted t_3. This is the residence time of the particle in Zone 3. The circulation time or total residence time is the sum of the elapsed times in each of the three zones and can be calculated as

$$T = t_1 + t_2 + t_3 \tag{22}$$

3. Materials and methods

3.1. Equipment

The predictions of the model were validated against output data taken from two separate experimental systems. The first (termed System A) is a simplified laboratory scale model of a re-circulatory fluidized bed unit. It is shown in Fig. 3. It consists of a 1.5 m tall Perspex outer tube of 150 mm diameter and a concentric inner tube of height 450 mm and diameter 50 mm. The base of the unit is a shallow conical steel mesh so a particle falling down through the outside region will fall in to the center and then be carried up the inner tube. Filter material of differing thickness was attached to the underside of the mesh to obtain a differential air velocity between the inner tube and outer annular zone and to promote uniformity of velocity within each zone. A centrifugal blower driven by an electric motor through a variable speed controller supplied air to the system. A number of unit spherical particles were obtained with diameters ranging from 2.33 mm up to 12 mm. These were coloured (for high visibility) had a smooth surface and were constructed from polypropylene with a density of 1044 kg/m^3.

While the fluidized bed unit of System A could not be used to carry out granulation trials, it was constructed specifically to facilitate validation of the kinematic output of the model. Its all-Perspex construction permits the position of the particles to be detected at all times and the straightforward flow geometry, corresponds very closely to the air flow model described in Section 2.1. The relatively large diameter test particles are easy to identify using the image analysis software. Also because of their large diameter, the Reynolds remains high for most of the motion meaning that the fluctuation in the drag coefficient from its time-averaged magnitude is low. This is needed for the analytical equations for particle velocity to be valid. Finally the almost perfect sphericity of the chosen particles allows a more reliable calculation of the drag coefficient.

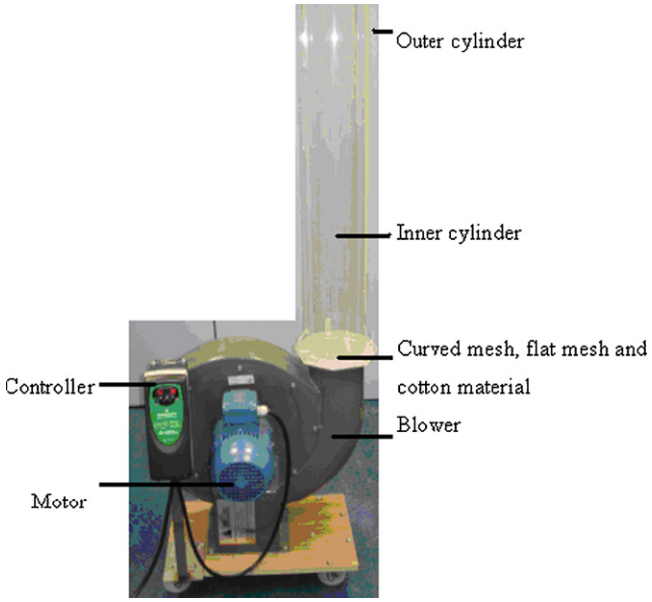

Fig. 3. Experimental simple re-circulatory fluidized bed unit (System A).

For a more realistic application of the validated theory, an actual laboratory-scale, fluidized bed granulator was analysed. The unit is a Procept granulator that can be configured to use the Wurster recirculation system. It is termed System B for this analysis and illustrated in Fig. 4. The equipment has an inner tube with a diameter of 45 mm and height of 200 mm. The base of the inner tube is 15 mm above the gas distributor plate. The main outer tube has a constant diameter of 100 mm up to an elevation 30 mm above the top of the inner tube. The form of the outer tube above that is that of an expanding cone frustum and it reaches a diameter of 200 mm at its maximum height of 700 mm above the distributor plate. The whole unit is can be dis-assembled into its components. The geometry and associated air flow pattern is more complex for this unit than for System A described above. Also the inner tube and constant diameter section of the main tube is built from stainless steel so the trajectory of the particle can only be monitored when it is within the glass conical section of the main tube. The particles fluidized in this unit are also more complex consisting of 250 μm diameter glass beads formed into granules (with typically 100 individual beads per particle) using poly-ethylene glycol (PEG) as the binder spray matrix. The spray nozzle is located halfway up the inner tube so the spray zone is taken to be the top half of the inner tube.

Fig. 4. Laboratory re-circulatory fluidized bed granulator (System B).

3.2. Measurement procedures

Initially an extensive series of experiments were conducted to measure air speed at a large number of locations within each unit to test how good an approximation the simplified three zone flow model is. For the laboratory granulator, the lower section of it was replaced with a plastic analogue of identical geometry to allow holes to be drilled in it for measurements. For each zone, air velocity in the vertical direction was measured at a number of radial positions and at a number of elevations. Air speed was measured with a number of different anemometers (moving vane, hot wire, pitot tube) to check for accuracy and repeatability. The values quoted in this paper are those taken with the hot wire anemometer. Note these measurements were taken without the presence of the fluidizing particles. The main reason for this is that the particles would break the measurement probe if impact between them occurred. It was assumed that for the very dilute fluidized beds under analysis here (porosity in excess of 98%), the effect of the particles on the air flow pattern would be negligible. For the simple re-circulatory unit, a number of smoke tests were also carried out with different smoke colours in the central and outer tubes to visually assess the air flow pattern.

The mass of each large plastic particle was measured with a Precisa mass balance and the diameter measured with a digital vernier. For these homogenous bodies, average density (Eq. (3)) is immediately known. For the real glass bead granules, equivalent diameter and sphericity were measured with the Pharmavision system, porosity measured by a pycnometer, mass using a mass balance and average mass fraction of PEG present in the granule using a dissolution bath. Density can then be calculated by Eq. (3). The drag coefficient of the various large spherical plastic particles used in the simple unit were measured and compared to the prediction of Eq. (6) as a check on the accuracy of the equations. Drag coefficient was measured by adjusting the blower speed so that the air velocity was sufficient to counteract the weight force and maintain the particle in an approximately stationary position. This air velocity corresponds to the particle terminal velocity and the turbulent drag factor and hence the drag coefficient could be obtained [10]. The values found by this technique (known as method 1) were compared to those found using a second subsidiary method which involved dropping the particles from rest in still air within a long Perspex tube and using light gates to quantify the elapsed time for a given displacement (method 2).

The main series of experiments were concerned with determining the displacement versus time histories of the different particles and granules in both pieces of equipment, the residence time in each zone and the total circulation time. These could then be compared to the analytical predictions. A high speed camera [AES] connected to displacement analysis software [MIDAS] was used to capture particle position at 500 frames per second, i.e. every 2 milliseconds. For System A, with large coloured particles that were relatively few in number, particle position was straightforward to identify and this was facilitated by using black paper behind the inner tube to block out any confusion from the downward moving particles in the rear of the annular space. For system, B the granule

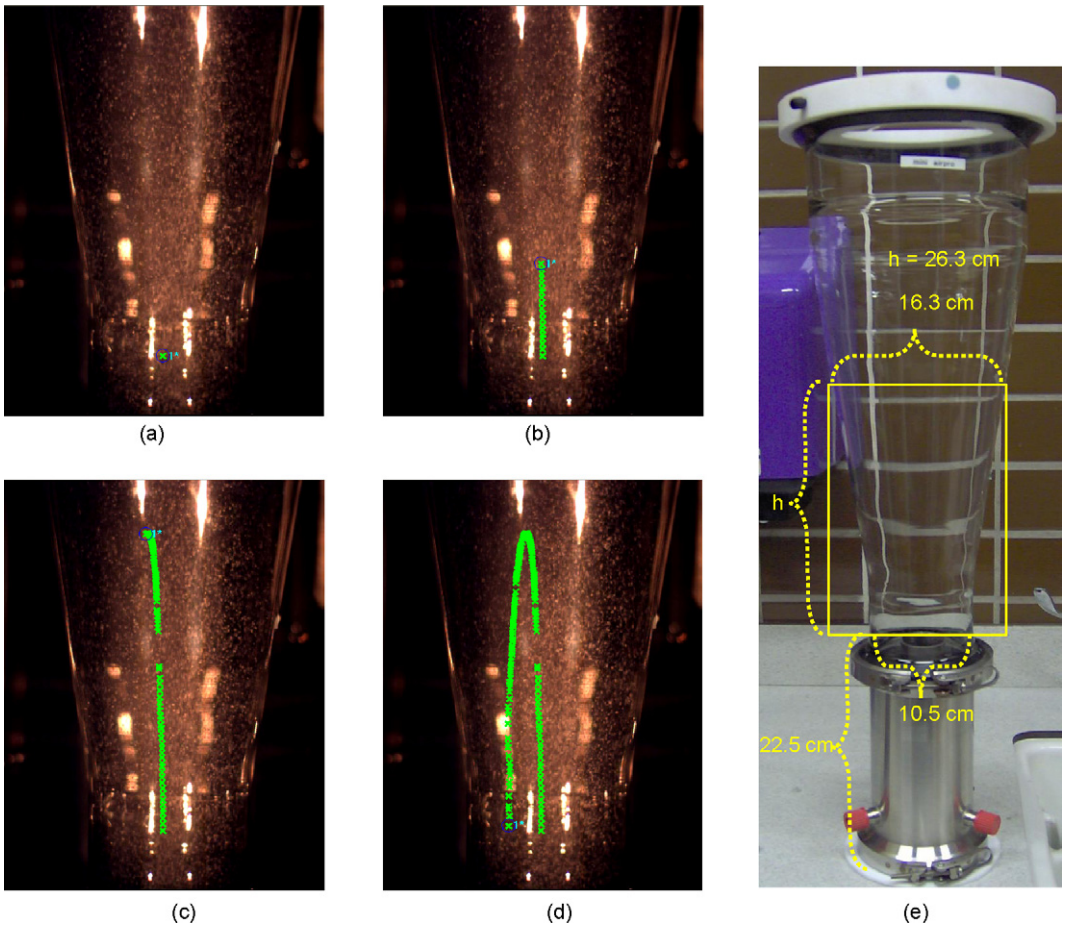

Fig. 5. Experimental determination of particle position.

to be tracked was painted with a colorant (Sudan Orange G, Sigma Aldrich) dissolved in the binder at a concentration of 1 mg/mL to aid identification. Fig. 5 illustrates how its position was monitored at various points throughout its motion commencing at exit from the top of the inner tube (Fig. 5a), to its apogee (Fig. 5c) and its return down the annular space (Fig. 5d). Fig. 5e illustrates the region of interest in the unit over which the displacement occurred.

The analytical equations (13)–(21) (based on an invariant magnitude for the drag coefficient) were coded in MATLAB so that analytical predictions of particle velocity and displacement versus time could be obtained. For the more numerical accurate model where the drag coefficient varied with the Reynolds number, the governing differential equation was solved with a 4th order Runge-Kutta solution scheme.

4. Results

4.1. Zone air velocities

For System A, analysis of the measured air velocities and the smoke test results indicated that air flow is axi-symmetric as expected. Measured air velocity varied rapidly with time (with a turbulence intensity of close to 15%) so in all cases time-averaged values are quoted. Increasing the blower speed, increases the air velocity in each zone and the overall flow pattern remains the same. The air flow pattern conformed quite well to that assumed in the model of three zones each described by a single, constant, uni-axial air velocity. This was found to be almost exactly the case for zone 1 (inner tube) and zone 3 (outer region of main tube) and the average measured air velocities are used as the model parameters. For zone 2 (central region of the main tube above the inner tube) the motion of the air is complex. Air speed in the vertical direction is spatially variable depending on radial and vertical position. The average value from the different measured locations was obtained and used to quantify zone air velocity.

System B (the Procept batch granulator) shared the basic flow characteristics of System A with an invariant air velocity in the inner tube and in the annular space between both tubes. In the main tube, above the inner tube, axial air velocity decreased rapidly with increasing elevation above the inner tube and within 80 mm approached an approximately constant value. As the upper main tube is conical in shape there is a radial component of air velocity present. Generally, though the resultant velocity vector is within 8° of the vertical axis so the radial term is small. Moreover it has little influence on the motion of the granules as was shown from experiment. One important effect that was noticed is that the motion of a particle in zone 2 depends on its radial position with respect to the vertical centerline of the unit. Granules emanating from the inner tube systematically reach higher elevations the closer they are to the center of the tube. Conversely granules that enter zone 2 from close to the side of the inner tube quickly reach maximum height and fall back. This effect can be included by considering air velocity above the inner tube in zone 2 to have a dependency on radial deviation from the unit vertical centerline. Knowing the radial location of the particle in the inner tube, the corresponding value of air velocity in zone 2 can be found. Thus the characteristic sprouting bed shape of the particles can be predicted. Table 1 summarises the air velocities used in each zone for both items of equipment.

Table 1
Zonal air velocities for both equipment systems.

Zone (–)	System A Air velocity (m/s)	System B (centerline) Air velocity (m/s)
1	12.19	7.32
2	6.5	2.7
3	5.67	0.52

4.2. Particle/granule kinetic properties

Table 2 contains the data for the spherical polypropylene particles used in System A. It gives the measured particle diameter, measured particle mass, terminal velocity and corresponding drag coefficient (by method 1) and the predicted drag coefficient (Eq. (6)) and corresponding Reynolds number. The final column gives the percentage error between the measured and predicted drag coefficient. In the calculation of Reynolds number, given that the air temperature was 20 °C; the density and viscosity of air were taken as 1.2 kg/m^3 and 1.8×10^{-5} Pa s, respectively. The drag coefficients measured by recording particle displacement versus time (method 2) were similar to the values found by measuring particle terminal velocity (method 1) though the data exhibited more variability.

As can be seen the agreement between the measured and predicted values of drag coefficient is good with the fractional difference being about 1% except for the 6.35 mm diameter ball where it is over 5%. This high level of agreement is taken to validate the accuracy of Eq. (6). With the high Reynolds numbers, drag coefficients are in all cases close to the limiting magnitude of 0.44. Table 3 contains the measured values of equivalent diameter, mass, sphericity and porosity for the granules of System B together with the calculated average density, drag coefficient and terminal velocity.

For the granules in this study, average binder content was low at 0.7% and hence makes very little contribution to density. As can be seen from the table, the granules are reasonably homogeneous in terms of physical and kinetic parameters. Average diameter is between 1 and 1.5 mm and drag coefficient can range from 0.5 up to 1. Fig. 6 displays a typical granule of such a system as displayed from the Pharmavision system.

4.3. Spherical particle displacement versus time—System A

Fig. 7 illustrates the measured displacement versus time for three replicated experiments and the calculated displacement versus time (analytical solution) for the 4 mm particle. There is good agreement between the theoretical prediction of particle displacement versus time and the measured values. Note the field of vision of the camera was obstructed by the curved mesh of the gas distributor near the base of the unit so experimental data is not presented at displacements less than 100 mm. The bottom of the inner tube corresponds to the zero displacement mark. The particle exits from the top of the inner tube (corresponding to a displacement of 450 mm) at a time in the region of 0.8 s. It travels upwards another

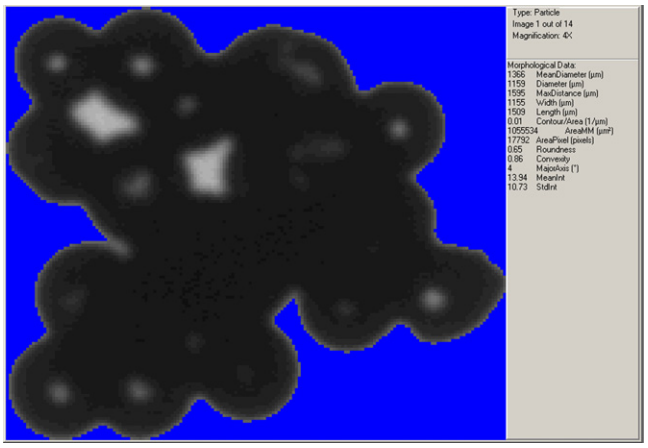

Fig. 6. Glass bead–PEG granule.

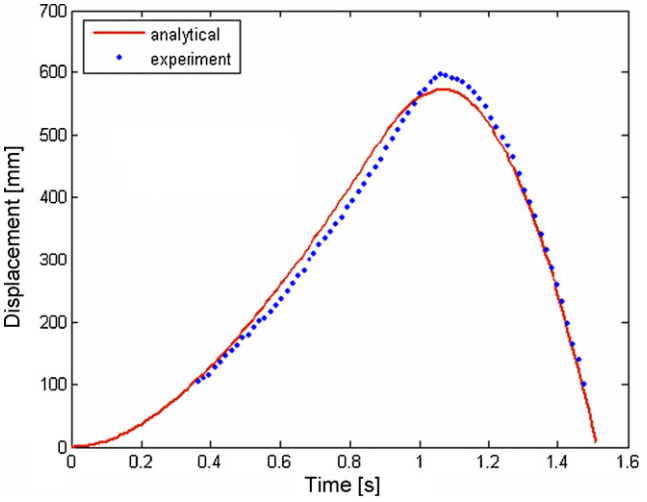

Fig. 7. Experiment, and analytical displacement versus time history for 4 mm spherical particle.

Table 2
Spherical particle kinetic properties.

d (mm)	m (mg)	u_T (m/s)	C_D (method 1) (–)	C_D (Eq. (6)) (–)	Re (–)	Difference (%)
2.33	7	7.88	0.44	0.432	1238	1.81
3	15	9.14	0.41	0.404	1820	1.46
4	34	10.61	0.39	0.389	2829	0.25
6.35	140	13.05	0.42	0.396	5524	5.71
12	985	17.7	0.44	0.436	14160	0.9

Table 3
Non-spherical granule kinetic properties.

Granule (–)	d_e (mm)	m (mg)	φ (–)	ε (–)	ρ (kg/m^3)	C_D (–)	u_T (m/s)
1	1.18	1.90	0.64	0.12	2165	0.95	5.47
2	1.20	2.00	0.73	0.14	2187	0.81	5.99
3	1.3	2.19	0.65	0.37	1488	0.93	5.38
4	1.37	2.20	0.91	0.3	1646	0.55	6.64
5	1.4	2.32	0.76	0.29	1608	0.76	5.69

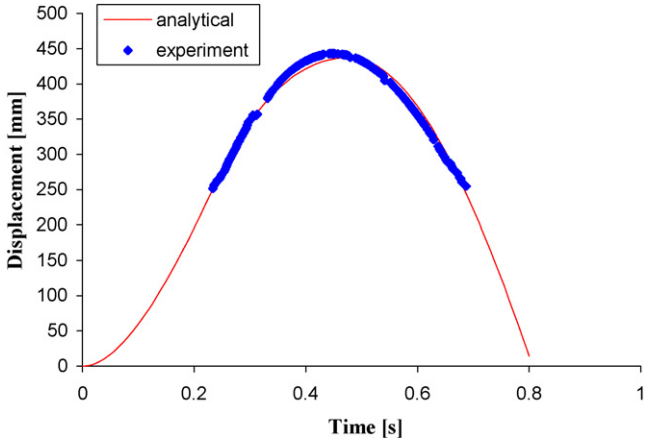

Fig. 8. Experiment and analytical displacement versus time history for Granule No. 3.

150 mm in the main tube and its maximum displacement at that point is just under 600 mm. At this point the elapsed time is nearly 1.1 s. It then falls back to zero displacement through the annular space between both tubes to the bottom of the system in a time of 0.4 s. Total circulation time is close to 1.5 s. The agreement between the analytical prediction (using a constant drag coefficient) and numerical prediction (where the drag coefficient was updated with particle velocity according to Eq. (6)) of displacement was also good as the time-averaged drag coefficient was found to lie between 0.41 and 0.44.

Overall agreement between theory and experiment was found to be good for all five particles of System A in terms of predicting residence time in each zone and recirculation time. Maximum error in the prediction of total or component residence time remained less than 10%. One outcome of the analysis demonstrated that circulation time is not very sensitive to particle diameter; this broadly reflects the fact that larger particles are carried more slowly up the inner tube but then fall faster down the outer tube.

4.4. Non-spherical granule displacement versus time—System B

Fig. 8 depicts the displacement versus time histories of granule number 3 (diameter 1.3 mm) whose properties were outlined in Table 3. The output from the experimental and analytical approaches are given. The experimentally measured displacement versus time is only available for part of the total motion for the reasons outlined in Section 3. The analytical solution used a constant value for the drag coefficient corresponding to the time-averaged Reynolds number for each granule in each zone; this was found by iteration of the solutions. Again the bottom of the inner tube corresponds to the zero displacement mark. The particle exits from the top of the inner tube (corresponding to a displacement of 230 mm for this system) at a time, t_1 just over 0.2 s. It travels upwards another 220 mm in the main tube and its maximum displacement at that point is about 450 mm. At this point the elapsed time is 0.45 s meaning residence time in zone 2, t_2 is also typically 0.2 s. It then falls back down to the base in a time. t_3 of 0.4 s. Total circulation time is close to 0.8 s.

One single parameter that represents granule motion quite well is the maximum elevation that it reaches. Table 4 gives the maximum height achieved for each of the granules as predicted by the model and experiment together with the fractional difference. As these granules are all similar in size and properties, the maximum height reached in zone 2, h_{max} is quite tightly bounded. The model predicts h_{max} very well and this provides evidence to validate both the granule kinetic model and the underlying air flow model. More generally when considering the behaviour of individual glass beads of 0.25 mm diameter up to granules of 2 mm diameter it was found that smaller particles achieve greater maximum heights in their sprouting motion and that his is a systematic effect. Individual glass beads achieved a maximum height of 580 mm above datum (365 mm above the top of the inner tube) while larger granules reached a height of 290 mm (70 mm above the inner tube). Also the smaller particles were seen to re-circulate faster through the system; perhaps four times a second while large granules circulated once a second.

Table 4
Non-spherical granule displacement output.

Granule	Experiment h_{max} (mm)	Model h_{max} (mm)	Difference (%)
1	444	432	2.78
2	459	463	0.86
3	438	436	0.46
4	445	450	1.11
5	261	265	1.51

5. Discussion

Analytical and numerical expressions for velocity and displacement for granules in a re-circulatory fluidized bed have been developed and validated. While the expression is not in a straightforward form, they do enable accurate predictions of residence time in the various zones of the system to be quantified. Most of their complexity is because particle velocity is not constant but is continually changing with time. In fact it can be shown that the assumption of constant particle velocity (equal to its terminal velocity plus or minus the local air velocity) that is sometimes reported in the literature is not valid for this system and would give erroneous results in the calculation of residence time. As an illustration, Table 5 compares the prediction of residence time in the inner tube, t_1 for the granules of System B, as calculated by Eq. (14) and as found by estimating the residence time with an assumption of steady-state velocity using

$$t_1 = \frac{h_1}{u_{F1} - u_{T1}} \tag{23}$$

As can be seen the error is significant with the simple approach markedly underestimating the time by an average factor of 2. In general (except for very small particles) any granule is subject to continuous acceleration over its re-circulatory motion and does not reach its constant asymptotic value in any zone.

Studies were also conducted to quantify the time-averaged Reynolds number in each of the flow zones for the particles and granules. Table 6 contains the results. Average Reynolds number for all zones and all bodies is greater for System A than for System B due to the larger diameter particles and the greater air velocities. In all cases though the Reynolds number is sufficiently high to justify the assumption that the drag force on the particle is essentially turbulent rather than laminar. For both systems, time-averaged Reynolds numbers are larger in Zone 1 (inner tube) than the other two zones. Larger average Reynolds numbers correspond to less relative fluc-

Table 5
Estimation of residence time in the inner tube.

Granule	Eq. (14) t (s)	Eq. (23) t (s)	Difference (%)
1	0.226	0.116	48.6
2	0.320	0.162	49.3
3	0.211	0.111	47.4
4	0.527	0.136	74.2
5	0.238	0.132	44.4

Table 6
Time-averaged Reynolds numbers.

System A				System B			
Particle	Zone 1	Zone 2	Zone 3	Granule	Zone 1	Zone 2	Zone 3
2.33 mm	1053.41	482.92	304.85	1.18 mm	347.66	154.76	78.29
3 mm	1657.36	772.54	519.99	1.2 mm	326.53	156.54	72.15
4 mm	2785.88	1359.20	854.14	1.3 mm	416.48	161.12	74.75
				1.37 mm	403.64	183.49	96.61
				1.4 mm	513.38	207.35	57.41

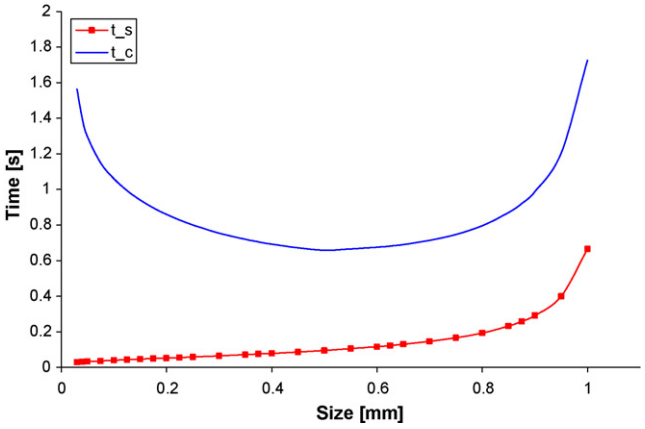

Fig. 9. Circulation time and spray zone residence time versus granule diameter.

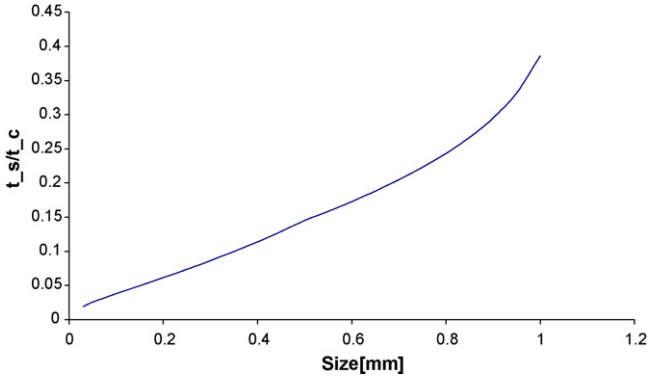

Fig. 10. Ratio of circulation time and spray zone residence time versus granule diameter.

tuation in the drag coefficient on the particle in the zone and mean the analytical formulae for velocity are more accurate.

The motion of a granule and hence its residence time in each system zone depends on a number of parameters including diameter, sphericity, porosity, average density and radial position in the inner tube. In a granulation operation, the most important parameter is diameter as the growth of this with time defines the progress of the operation. Quantifying how spray zone residence time and total recirculation time of a granule depend on its diameter may permit the granulation characteristics of a system to be assessed. Granule wetting, collision and hence granulation are much more likely to occur in the spray zone than in other zones. So the spray zone residence time gives a measure of the duration of active processing of the granule while the remainder of the circulation time can be considered as a passive transport phase. According to this the granule diameter (size) that has the maximum ratio of these times would be expected to agglomerate fastest.

Fig. 9 gives a plot of the residence time in the spray zone, t_S and total recirculation time, t_C in the range from 0.03 mm up to 1 mm as obtained from the kinetic model. Note all other granule properties (binder content, sphericity, porosity) are held constant at $x_B = 0.007$, $\varphi = 0.8$, $\varepsilon = 0.3$. Total circulation time exhibits a minimum with respect to diameter; this arises because small granules have a long residence time, t_3 falling through the outer annular region (zone 3) due to their low terminal velocity while conversely large granules have a long residence time in the inner tube (zone 1) because their large terminal velocity is closer in magnitude to the upwards fluid velocity, u_{F1}. For the data of this paper, a granule with a diameter of 0.5 mm has the lowest circulation time and for a given batch processing time (typically of the order of 20 min) makes the most circulations through the system. This finding for t_C is also consistent with result that have been reported by Tan et al. [10]. A particle size that has a minimum circulation time has by definition a maximum average velocity in the domain and the distribution in velocity would be bell-shaped similar to the Gaussian distribution. Residence time in the spray zone, t_S monotonically rises with granule diameter as larger granules take longer to pass through the top half of the inner tube.

Fig. 10 displays the ratio t_S/t_C versus granule diameter. The ratio continually increases; at a rapid rate at very low values of diameter, more slowly for the mid-range diameters and then rapidly again for the large diameter granules. Thus the larger the diameter of the granule, the greater is the fraction of its circulation time that it spends in the active zone. Given total processing duration is fixed for batch granulation, the larger this ratio is the longer the absolute time a granule spends in the spray zone. The thrust of this argument is that the larger the granule, the more readily it should agglomerate and granulation growth should accordingly be exponential with time. However granulation dynamics are complex, involving many factors in addition to system residence times. For some of these subprocesses, granulation rate is inversely related to granule diameter and may counteract the above effect.

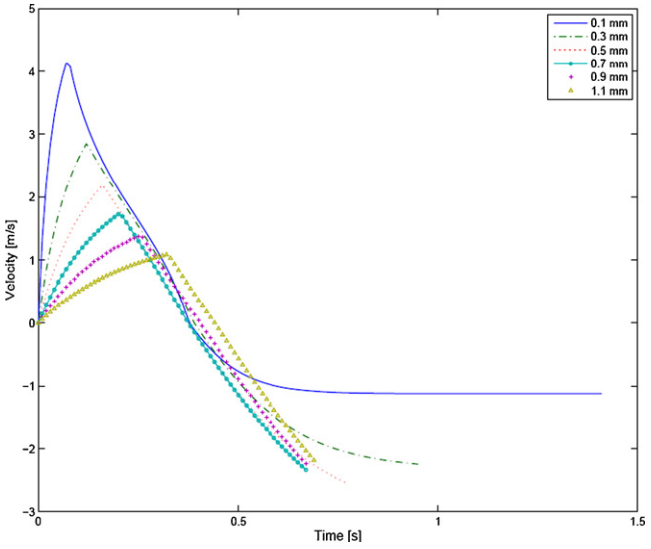

Fig. 11. Velocity versus time histories of different sizes of granules.

Finally Fig. 11 illustrates velocity versus time profiles as predicted by the model for five different sized granules within the diameter range examined above. Initial velocity is zero for all the granules and maximum velocity is achieved as the granules exit the top of the inner tube. The velocity falls back to zero again at the point of maximum elevation of the granules. After that velocity is negative as the granules fall down to return to the starting position. There is a continuous variation in velocity for each granule and a large difference in velocity of granules of different size. Small granules experience the highest velocity of the motion at the top of the inner tube (zone 1) while large granules achieve greatest velocity at the base of the outer region (zone 3). This information can be utilized to determine the zones where agglomeration of small particles and breakage of large granules are likely to occur.

6. Conclusions

A model of particle and granule kinetics in a re-circulatory fluidized bed unit has been developed and validated. Motion of the particles in the system is determined by the respective magnitudes of weight force and drag force in the various zones of the system. Determination of the drag force requires both knowledge of granule physical characteristics and air velocity in each zone. The analysis demonstrates that a simplified flow model can realistically represent the more complex real flow pattern at least as far as predicting granule motion. Having expressions for granule velocity and displacement versus time, enables residence time of particles in the system to be calculated. Studies with the model demonstrate that the time varying nature of granule velocity must be taken into account when estimating residence time; treating velocity as constant leads to erroneous predictions. Also the sensitivity of residence time to granule diameter can be discerned. One further advantage of having analytical expressions for particle motion, is that it enables the influence of zone air velocity on the motion to be more easily identified. This can permit strategies to select these zonal velocities to minimize the variation in circulation time of different sized granules to be selected or to promote more uniformity in granule velocity in each zone. The experiments conducted in association with this work revealed that there is considerable dispersion in the recirculation time of the particles. This is due to systematic spatial variation in air velocity, high frequency temporal fluctuations in air velocity, particle to wall collisions and inter-particle collisions. The experiments also indicated that average residence time becomes longer as the number of particles that are circulating increases. Future work will involve incorporating these effects into the velocity model.

Acknowledgements

This publication has emanated from research conducted with the financial support of Science Foundation Ireland.

References

[1] F. Ronnse, J.G. Pieters, K. Dewettinck, Numerical spray model of the fluidized bed coating process, Drying Technology 25 (2007) 1491–1514.
[2] S. Heinrich, L. Morl, Fluidized bed spray granulation—a new model for the description of particle wetting and of temperature and concentration distribution, Chemical Engineering and Processing 38 (1999) 635–663.
[3] E. Teunou, D. Poncelet, Batch and continuous fluid bed coating—review and state of the art, Journal of Food Engineering 53 (2002) 325–340.
[4] A.T. Harris, R.B. Thorpe, J.F. Davidson, Stochastic modeling of the particle residence time distribution in circulating fluidized bed risers, Chemical Engineering Science 57 (2002) 4779–4796.
[5] J.P.K. Seville, U. Tuzun, R. Clift, Processing of Particulate Solids, Kluwer, 1997 (Chapter 3).
[6] J. Li, D. Mason, Application of the discrete element modeling in air drying of particulate solids, Drying Technology 20 (2002) 255–282.
[7] M. Li, P.D. Christofides, Modeling and analysis of HVOF thermal spray process accounting for powder size distribution, Chemical Engineering Science 58 (2003) 849–857.
[8] R. Turton, O. Levenspiel, A short note on the drag coefficient for spheres, Powder Technology 47 (1986) 83–86.
[9] G.H. Ganser, A rational approach to drag prediction of spherical and nonspherical particles, Powder Technology 77 (1993) 143–152.
[10] H.S. Tan, M.J.V. Goldschmidt, R. Boerefijn, M.J. Hounslow, A.D. Salman, J.A.M. Kuipers, Building population balance model for fluidized bed melt granulation: lessons from kinetic theory of granular flow, Powder Technology 142 (2004) 103–109.